Monthly Notices
of the
ROYAL ASTRONOMICAL SOCIETY

Mon. Not. R. Astron. Soc. **403,** 605–619 (2010) doi:10.1111/j.1365-2966.2009.16146.x

Twelve years of X-ray and optical variability in the Seyfert galaxy NGC 4051

E. Breedt,[1⋆] I. M. McHardy,[1] P. Arévalo,[2,3] P. Uttley,[1] S. G. Sergeev,[4,5] T. Minezaki,[6] Y. Yoshii,[6,7] Y. Sakata,[8] P. Lira[9] and N. G. Chesnok[10,11]

[1]*School of Physics and Astronomy, University of Southampton, Southampton SO17 1BJ*
[2]*Shanghai Astronomical Observatory, 80 Nandan Road, Shanghai 200030, China*
[3]*Departamento de Ciencias Fisicas, Universidad Andres Bello, Av. Republica 252, Santiago, Chile*
[4]*Crimean Astrophysical Observatory, P/O Nauchny, Crimea 98409, Ukraine*
[5]*Isaac Newton Institute of Chile, Crimean Branch, P/O Nauchny, Crimea 98409, Ukraine*
[6]*Institute of Astronomy, School of Science, University of Tokyo, 2-21-1 Osawa, Mitaka, Tokyo 181-0015, Japan*
[7]*Research Centre for the Early Universe, School of Science, University of Tokyo, 7-3-1 Hongo, Bunkyo-ku, Tokyo 113-0033, Japan*
[8]*Department of Astronomy, School of Science, University of Tokyo, 7-3-1 Hongo, Bunkyo-ku, Tokyo 113-0033, Japan*
[9]*Departamento de Astronomía, Universidad de Chile, Casilla 36-D, Santiago, Chile*
[10]*Taras Shevchenko National University of Kiev, pr. Akademika Glushkova 2, Kiev 03680, Ukraine*
[11]*Main Astronomical Observatory, Ukrainian National Academy of Sciences, ul. Akademika Zabolotnogo, 27, Kiev 03680, Ukraine*

Accepted 2009 December 2. Received 2009 December 1; in original form 2009 August 3

ABSTRACT

We discuss the origin of the optical variations in the narrow-line Seyfert 1 galaxy NGC 4051 and present the results of a cross-correlation study using X-ray and optical light curves spanning more than 12 years. The emission is highly variable in all wavebands, and the amplitude of the optical variations is found to be smaller than that of the X-rays, even after correcting for the contaminating host galaxy flux falling inside the photometric aperture. The optical power spectrum is best described by an unbroken power-law model with slope $\alpha = 1.4^{+0.6}_{-0.2}$ and displays lower variability power than the 2–10 keV X-rays on all time-scales probed. We find the light curves to be significantly correlated at an optical delay of $1.2^{+1.0}_{-0.3}$ d behind the X-rays. This time-scale is consistent with the light traveltime to the optical emitting region of the accretion disc, suggesting that the optical variations are driven by X-ray reprocessing. We show, however, that a model whereby the optical variations arise from reprocessing by a flat accretion disc cannot account for all the optical variability. There is also a second significant peak in the cross-correlation function, at an optical delay of $39^{+2.7}_{-8.4}$ d. The lag is consistent with the dust sublimation radius in this source, suggesting that there is a measurable amount of optical flux coming from the dust torus. We discuss the origin of the additional optical flux in terms of reprocessing of X-rays and reflection of optical light by the dust.

Key words: galaxies: active – galaxies: individual: NGC 4051 – galaxies: Seyfert.

1 INTRODUCTION

The exact mechanism producing the X-ray emission from active galactic nuclei (AGN) is not well understood, although most models involve Comptonization of the UV/optical spectrum, through a tenuous, hot corona above the inner disc (Haardt & Maraschi 1991). The fastest variability time-scales set a limit on the size of the emission region, suggesting that the X-rays are emitted from the innermost regions of the system, but the exact geometry is not known. The optical continuum is variable as well and thought to be thermal emission from an optically thick accretion disc, surrounding the black hole (Koratkar & Blaes 1999). The origin of the variability, as well as the connection between the disc and the corona, is still unclear, however. It has been suggested that the short time-scale optical variations are the result of reprocessing of the highly variable X-rays by the disc (Krolik et al. 1991), enhancing the intrinsic thermal emission from the disc. Hence, variations in the X-rays should be mirrored in the optical light curves, smoothed by the large size of the disc and delayed by the light traveltime between the source and the disc. Although there are some sources that do show evidence of reprocessing (e.g. Wanders et al. 1997; Collier et al. 1998; Oknyanskij et al. 2003; Sergeev et al. 2005; Cackett, Horne & Winkler 2007), the results are not generally applicable.

⋆E-mail: ebreedt@astro.soton.ac.uk

Many sources show no simple relationship between bands (Nandra et al. 2000; Gaskell 2008) and at least one source shows no correlation at all (Maoz, Edelson & Nandra 2000; Maoz et al. 2002). An increasing number of sources display optical variations of greater amplitude than their corresponding X-ray variations, such as NGC 5548 (Uttley et al. 2003), MR 2251-178 (Arévalo et al. 2008), Mrk 79 (Breedt et al. 2009) and NGC 3783 (Arévalo et al. 2009), making it difficult to attribute all the optical variability to reprocessing. Energetics arguments also rule out reprocessing as the main driver of the variability in sources where the variable optical luminosity exceeds the X-ray luminosity (Gaskell 2007).

Also important to consider is variability intrinsic to the disc, such as instabilities propagating radially inwards through the disc, affecting the mass accretion rate and local emission (e.g. Lyubarskii 1997). In this case, optical variations are expected to precede similar variations in the X-rays. The time-scales involved are much longer, as variations will propagate on the viscous time-scale, which is of approximately months to years at the optical emitting region in AGN.

The long-term (approximately months to years) optical variability has been explained by composite models including accretion rate fluctuations propagating through the disc (Arévalo & Uttley 2006; Arévalo et al. 2008) and changes in the geometry of the system (Breedt et al. 2009). Reprocessed emission from the broad-line region (BLR) may also contribute to the optical variations (Korista & Goad 2001; Arévalo et al. 2009), and Gaskell (2007) suggested that there might be a contribution to the optical emission from reprocessing material much further out, such as the molecular torus.

By undertaking simultaneous multiwavelength monitoring and studying the correlation between the emission at different wavelengths, we can determine the dominant process underlying the optical variations and gain some physical insight into the connection between the emission regions.

Uttley et al. (2003) proposed that the dominant process driving the observed optical variability was dependent on the mass and accretion rate of the black hole, as these parameters define the temperature profile of the accretion disc. Within the standard accretion disc model (e.g. Shakura & Sunyaev 1973), AGN with smaller black hole mass and/or higher accretion rate will have hotter discs than systems with a high mass/low accretion rate. Scaled in terms of the gravitational radius, the X-ray and optical emitting regions are further apart in the low mass systems, so the viscous time-scale in the optical emitting region is very long compared to that in the inner disc. We may therefore expect reprocessing to be the main contributor to the fast optical variations and accretion rate variations to occur on time-scales of several tens of years.

NGC 4051 is a low-luminosity narrow-line Seyfert 1 galaxy, known for its extreme X-ray variability (e.g. McHardy et al. 2004). The relationship between the X-ray and UV/optical variability in this galaxy has been the subject of many papers, reporting varied and conflicting results. Over the course of three nights Done et al. (1990) found the X-rays to vary by a factor of 2, but no corresponding variations in the optical or infrared were seen. Klimek, Gaskell & Hedrick (2004) also studied the short time-scale optical variability of this galaxy. They detected microvariability on one of the five nights it was observed. Uttley et al. (2000) found a strong correlation between the X-ray and extreme UV (EUV) variations and measured them to be simultaneous to within 1 ks. Peterson et al. (2000) concluded that the X-ray and optical emission was correlated on time-scales of months to weeks, but by applying a 30 d smoothing boxcar to the light curves before calculating the cross-correlation, a measurement of any lag shorter than this could not be obtained. During a period of very low X-ray flux, they found that the broad He II λ4686 line greatly decreased in intensity as well, showing no noticeable variation during this period, but that the optical continuum and Hβ line were only slightly fainter and continued to vary. They interpreted this as the inner disc turning into an advection-dominated flow, greatly reducing the short wavelength (UV/blue) emission from this part of the disc. A 3 month simultaneous X-ray and optical monitoring programme by Shemmer et al. (2003) revealed significant evidence of a correlation close to zero lag. They found the optical emission in this case to *lead* the X-ray emission by 2.4 d and noted that the variability of the optical light curve was much less than that of the X-rays. On shorter time-scales, Mason et al. (2002) find the UV to lag the X-rays, which they interpret as reprocessing by a ring of material at a distance of 0.14 light-days. This result has also been confirmed by Smith & Vaughan (2007), using the same data. Reverberation mapping studies using the Hβ line (Kaspi et al. 2000; Peterson et al. 2000, 2004) place the BLR in this AGN at a distance of $\sim$6 light-days from the central ionizing source.

It is clear that a combination of processes can contribute to the observed optical variability and that different processes can drive the variability on different time-scales. In this paper, we combine the observations from four different telescopes with some archival data, to revisit the topic of X-ray and optical variability in NGC 4051. The light curves together span more than 12 years, allowing us to study the variability on much longer time-scales than has been done before in this source. This paper is the fourth in a series describing our findings from a sample of Seyfert galaxies monitored at X-ray and optical wavelengths. Previously we have reported on our results on MR 2251-178 (Arévalo et al. 2008), Mrk 79 (Breedt et al. 2009) and NGC 3783 (Arévalo et al. 2009) and here we discuss our findings on NGC 4051, the lowest mass [$M = (1.91 \pm 0.78) \times 10^6\,\mathrm{M}_\odot$; Peterson et al. 2004], lowest luminosity ($L_{\rm bol} < 10^{44}\,\mathrm{erg\,s^{-1}}$) galaxy in our sample. Throughout, we adopt the average Tully–Fisher distance estimate of 15.2 Mpc (Russell 2003) to this source.

In Section 2, we present the multicolour optical and X-ray data. We show the optical power spectrum in Section 3, and in Section 4 we present the results of a cross-correlation analysis of the light curves. We discuss the results in terms of a simple reprocessing model in Section 5 and show that there is an additional component to the optical variability. We show that these additional variations are delayed with respect to the X-rays by a time-scale consistent with the light traveltime to the torus, so in Section 6 we investigate the possibility of optical emission originating from the torus, in detail. Our findings are summarized in Section 7.

2 DATA

2.1 *V*-band optical observations

The *V*-band optical light curve presented in this paper is a combined light curve from four telescopes: the Liverpool Telescope (LT) at the Observatorio del Roque de Los Muchachos of the Instituto de Astrofisica de Canarias, La Palma, Spain[1] (Steele et al. 2004); the Faulkes Telescope North (FT) at Haleakala, Maui, Hawaii; the Multicolor Active Galactic Nuclei Monitoring (MAGNUM) telescope (Yoshii, Kobayashi & Minezaki 2003) at the University of Hawaii's

[1] The Liverpool Telescope is operated by Liverpool John Moores University with financial support from the UK Science and Technology Facilities Council.

Haleakala Observatory, Maui, Hawaii; and the 0.7-m telescope of the Crimean Astrophysical Observatory (CrAO) in Crimea, Ukraine (Sergeev et al. 2005; Chesnok, Sergeev & Vavilova 2009). The data reduction procedures and light-curve construction are described in detail in Breedt et al. (2009), so we only give a brief summary below.

We observed NGC 4051 through a Bessell V-band filter from 2004 December 9 to 2008 December 11 with the LT and from 2007 February 5 to 2007 August 10 with the FT North. The two telescopes are identical in design. Observations in other filter bands, on both telescopes, started in early 2007 and continued until 2007 August on the FT and 2008 July on the LT. The data reduction and photometry were done using standard techniques in IRAF. We performed aperture photometry on the individual images, using an aperture of 12 arcsec diameter, centred on the nucleus of the galaxy. The relative fluxes were calibrated with respect to four comparison stars in the field and the final flux calculated using the comparison star magnitudes of Doroshenko et al. (2005).

The MAGNUM telescope observed NGC 4051 in the V band from 2001 January 8 to 2007 July 30. Data from the start of this programme until MJD 52819 (2003 June 29) have been published by Suganuma et al. (2006). The rest of the light curve was previously unpublished.

Observations at the CrAO were carried out between 2001 December 27 and 2006 August 18. The filter set on the Crimean telescope is non-standard, but their B, V, R and I filters are close to the Johnson/Bessell filters and their $R1$ filter is similar to the Cousins I filter (see Doroshenko et al. 2005).

The light curves from the different telescopes were made using different aperture sizes, so each is affected by a different amount of host galaxy contamination, resulting in different average flux levels. To account for this, as well as for the slight differences in the filters and any other small systematic differences in the calibration, we use the overlapping parts of the light curves to match them in a least-squares fashion. We extracted pairs of measurements, taken within 1 d of each other, from overlapping light curves, and performed a least-squares fit of the equation $F_1 = aF_2 + b$ to the flux pairs. F_1 and F_2 are the flux measurements from the two data sets and a and b the parameters of the fit. The points were weighted for the fit, by the inverse of the time difference between F_1 and F_2, so that measurements made closer together in time have a greater influence on the fit. The best-fitting parameters from each pair of overlapping light curves were then used to scale that data set to the 15 arcsec diameter aperture V-band light curve from the CrAO telescope.

The V-band light curve used in the analysis is the final combined light curve, corrected for Galactic reddening and host galaxy flux inside the aperture (see Section 2.5). It is shown in Fig. 1, normalized to its mean flux, for direct comparison with the X-ray variations. Full sampling characteristics of this light curve may be found in Table 1.

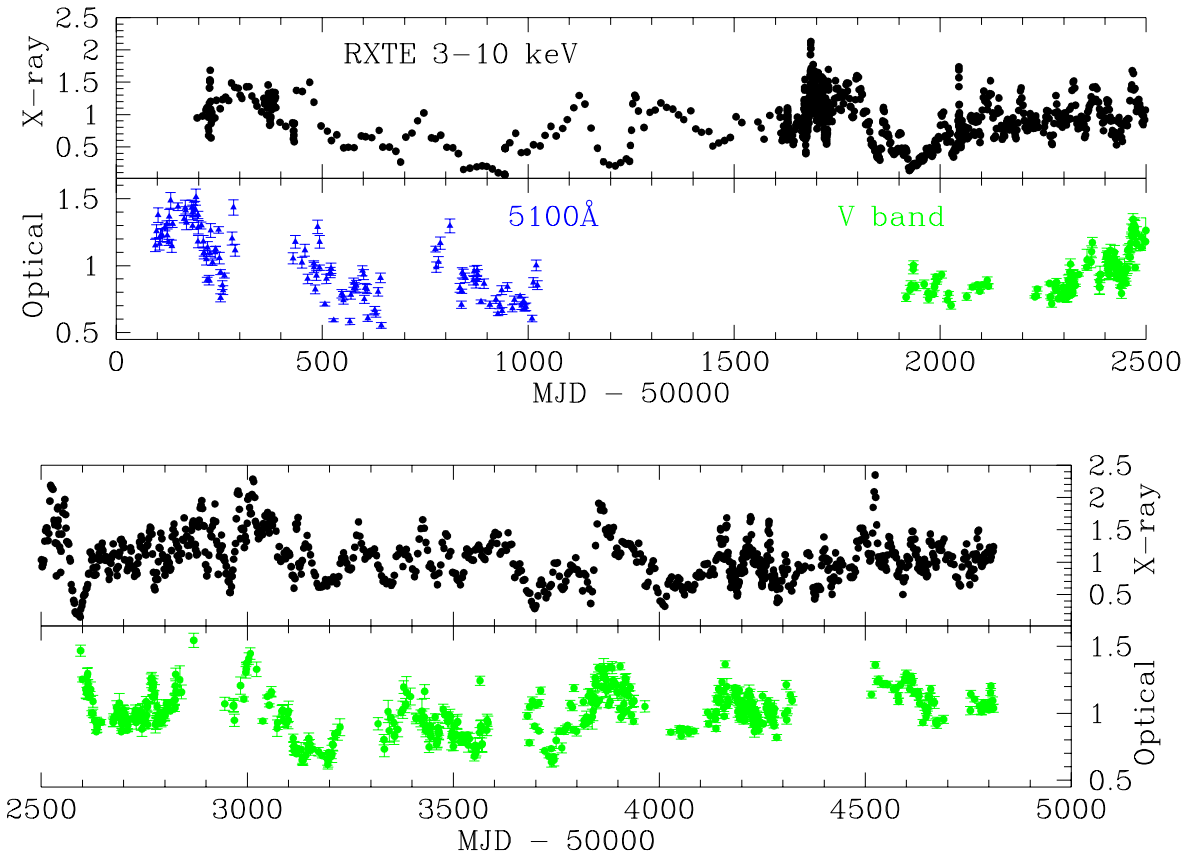

Figure 1. 3–10 keV X-ray (top panel in each part) and optical (bottom panel in each part) light curves of NGC 4051, corrected for host galaxy flux inside the aperture. Each light curve is normalized to its mean flux for direct comparison of the variability amplitudes. Note that the vertical scales for the optical and X-ray light curves are different – the amplitude of the optical variations is smaller than that of the X-rays. The X-ray light curve is smoothed with a four-point (∼1 week) running average (for plotting purposes only), to highlight the variations on time-scales similar to those of the optical light curve. The first part of the optical light curve, plotted in blue triangles, is the 5100 Å continuum light curve from the AGN Watch programme. The rest of the light curve, plotted in green dots, is the combined V-band light curve from four different telescopes.

Table 1. Observational characteristics of all light curves.

Light curve	Telescope	Observation dates (MJD)	Total length (d)	Number of epochs	$\Delta t_{\rm mean}$ (d)	$\Delta t_{\rm median}$ (d)	Mean flux[a] (mJy)
X-ray	*RXTE*	50196–54811	4615	1811	2.55	1.96	1.93 ± 0.95^{b}
u	LT	53348–54675	1327	128	10.4	4.01	5.41 ± 0.93
B	Combined	52271–54675	2404	386	6.24	1.96	11.5 ± 0.61
5100 Å	AGN Watch	50095–51023	928	126	7.42	3.15	11.1 ± 0.93
V	Combined	51917–54811	2894	629	4.61	1.94	20.1 ± 0.64
R	Combined	52271–54675	2404	384	6.28	1.97	32.3 ± 0.91
*R*1[c]	CrAO	52271–53965	1694	265	6.42	1.98	38.9 ± 1.02
I	CrAO	52271–53965	1694	261	6.52	1.98	41.3 ± 1.02

[a]Including the host galaxy flux.
[b]In units of 10^{-11} erg s^{-1} cm^{-2}.
[c]The *R*1 filter corresponds approximately to the Cousins *I* filter.

2.2 AGN Watch continuum light curve

NGC 4051 was also observed spectroscopically between 1996 January 12 and 1998 July 28 as part of the International AGN Watch programme (e.g. Peterson 1999). Light curves from this programme are publicly available[2] and we include in our analysis the 5100 Å continuum light curve originally presented by Peterson et al. (2000). We subtracted the host galaxy contribution inside the 5.0×7.5 arcsec^2 spectroscopic aperture, as measured by Bentz et al. (2009), and converted the light curve to mJy units, to compare with our *V*-band light curve. Note that in this light curve the continuum flux is measured from a line-free region around 5100 Å of the optical spectra, while the broad-band observations will contain the line emission that falls inside the *V*-band bandpass, such as [O III] λλ4959, 5007 and Hβ λ4861. We discuss the contribution of the lines to the flux in Section 4.1. The light curve is plotted in Fig. 1, together with the X-ray and *V*-band light curves.

2.3 Multicolour optical observations

In addition to the *V*-band observations described above, the CrAO also observed NGC 4051 in the *B*, *R*, *R*1 and *I* filter bands during the same period. The light curves are constructed from aperture photometry through a 15 arcsec diameter aperture centred on the galaxy nucleus, relative to a comparison star in the field. We use the comparison star fluxes from Cackett et al. (2007) to convert the light curves to flux units in these bands. The data from the start of this programme, until MJD 53022 (2004 January 18), have been published by Sergeev et al. (2005) and were also analysed by Cackett et al. (2007). Data after this date were previously unpublished.

We supplement these light curves with Sloan Digital Sky Survey (SDSS)-*u*-band observations made by the LT between 2004 December 9 and 2008 July 27. The data from short monitoring programmes in *B* and *R* on the LT and FT (2007 February 5–2008 July 27) were combined to extend the CrAO light curves. Unfortunately there is no overlap between the LT/FT and the CrAO light curves in these bands, so it was not possible to combine them as described in Section 2.1. To ensure the best possible match between the light curves, the same comparison stars were used in the flux calibration of the two data sets, and the appropriate aperture corrections were applied to the LT/FT light curves. However, it is possible that small differences in the calibration, or between the filters on the different telescopes, may cause a small offset between the CrAO and LT/FT light curves. The positions in the light curves that are affected by this are indicated by dotted lines in Fig. 2. Note, however, that due to the 'segmentation' technique we use to calculate the cross-correlation (Section 4), a possible small offset like this does not affect our results. The light curves are shown, together with the corresponding segment of the X-ray light curve, in Fig. 2.

The flux uncertainty on each point, based upon the differential photometry error and the relative calibration of the light curves, is approximately 3 per cent. The uncertainty in the comparison star fluxes introduces a 1–4 per cent error in average flux of the different bands, but note that this error does not increase the scatter in the light curve, so it does not affect the cross-correlation results below. Sampling statistics for each light curve are shown in Table 1.

2.4 X-ray observations

NGC 4051 is part of our long-term AGN X-ray monitoring programme using *Rossi X-Ray Timing Explorer* (*RXTE*), which started on 1996 April 23. Here we include the observations up to 2008 December 11, to overlap with the optical light curve. The observational frequency and variability characteristics of this light curve are summarized in Tables 1 and 2, respectively. The observations are in the form of approximately 1 ks snapshots using the proportional counter array (PCA) on board *RXTE*. The PCA consists of five identical proportional counter units (PCUs) but as some of them were regularly switched off during our observations, we only extracted data from PCU2 to construct the X-ray light curve. For a maximum signal-to-noise ratio, we used only the data from the top layer. Using FTOOLS v.6.4, we applied standard extraction techniques and re-reduced all the available data so that the latest *RXTE* background models may be applied throughout the light curve. We rejected data obtained within 10 min of passing through the South Atlantic Anomaly, data gathered less than 10° above the limb of the Earth or with pointing offset greater than 0.°02 from the source, and data for which the electron current was greater than 10 per cent. To obtain the flux measurement, we fit a power-law model to the spectra using XSPEC and integrate the flux in the range of 3–10 keV. The error on the flux measurements was calculated from the counts in each observed spectrum, weighted by the response function.

We show the normalized 3–10 keV X-ray light curve in Fig. 1, smoothed with a four-point (∼1 week) running average. This is done to highlight fluctuations on similar time-scales as those in the optical light curve, but note that, throughout this paper, the unsmoothed, unbinned light curve was used in the analysis.

[2] http://www.astronomy.ohio-state.edu/∼agnwatch/

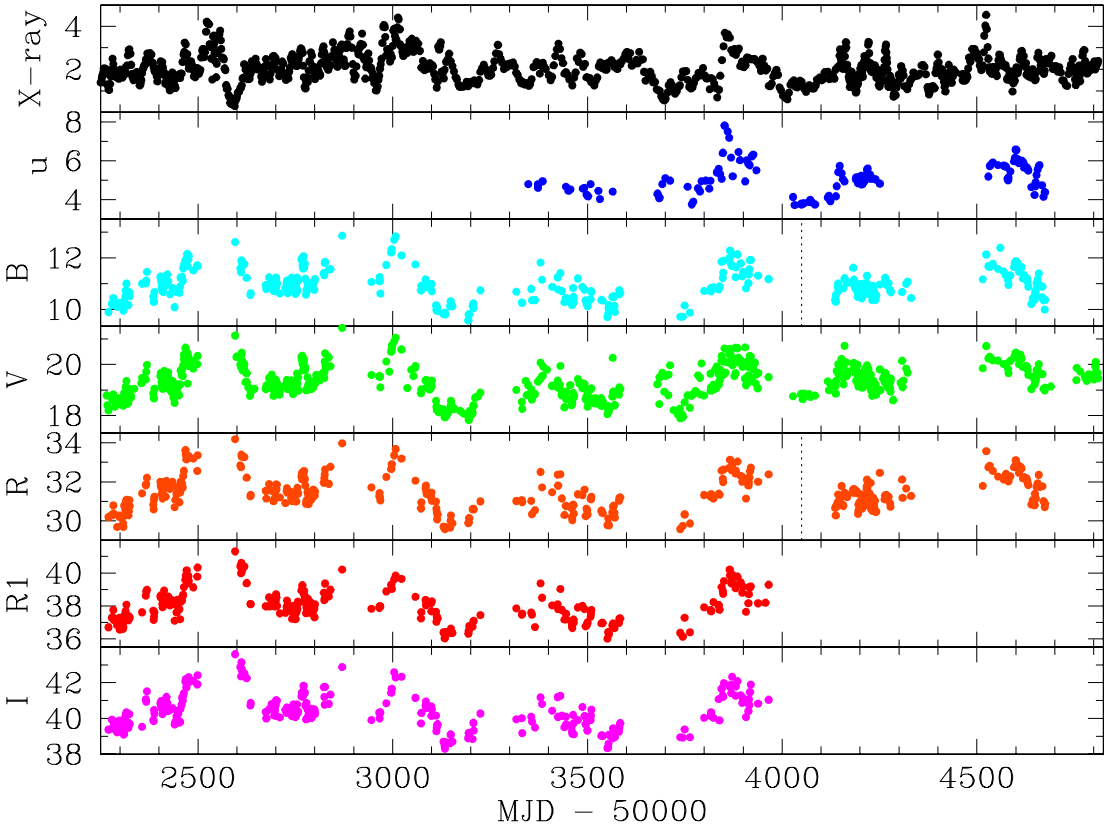

Figure 2. X-ray, *u*-, *B*-, *V*-, *R*-, *R*1- and *I*-band light curves of NGC 4051. The X-ray light curve is in units of 10^{-11} erg s^{-1} cm^{-2} and the optical light curves are in mJy. The fluxes have been corrected for the small amount of Galactic extinction towards the source, but the host galaxy flux has not been subtracted. The dotted lines in the *B*- and *R*-band light curves indicate the positions where there might be a small offset between the light curves on either side of the line, as there was no overlap between the data from the different telescopes. This does not affect our cross-correlation results however (see text).

Table 2. Estimated host galaxy flux inside the 15 arcsec aperture and variability characteristics of all light curves, after subtracting the host galaxy contribution.

Light curve	f_g (mJy)	F_{var} (per cent)	f_{max}/f_{min}
X-ray	–	48.8 ± 0.8	89.0 ± 26.5
u	1.8	25.6 ± 1.8	3.92 ± 1.36
B	6.3	11.7 ± 1.5	1.92 ± 0.56
V	16.0	15.4 ± 3.1	2.48 ± 1.64
R	27.2	16.9 ± 3.8	2.46 ± 1.65
*R*1	31.5	13.8 ± 3.3	2.02 ± 0.92
I	32.7	11.8 ± 3.0	1.84 ± 0.72
5100 Å	7.2[a]	23.9 ± 1.5	2.73 ± 0.15

[a]Bentz et al. (2009), in the 5.0×7.5 arcsec^2 spectroscopic aperture.

2.5 Galaxy flux in the aperture

The photometry aperture contains the nuclear emission as well as a constant contribution from stars in the host galaxy. Although this constant offset does not affect the results of the cross-correlation analysis, it reduces the amplitude of the observed variations. Hence, to investigate the variability of the nucleus, this component must be subtracted from the light curve.

In order to estimate the amount of host galaxy flux contained in the 15 arcsec aperture, we decomposed the images using GALFIT (Peng et al. 2002), by fitting a point spread function (PSF; using stars in the field of the galaxy), a de Vaucouleurs profile and an exponential disc to each image. The decomposition of individual images was poor, so we stacked together 12 images taken under good seeing conditions, to improve the signal-to-noise ratio. This resulted in much better, stable fits of the different components. The variable nucleus was taken account of by selecting only images from which we measured approximately the same flux through the aperture. We subtracted the best-fitting galaxy profile in each band from the images and measured the flux of the residual PSF-like image. The difference between this PSF-like image and the flux measured through a 15 arcsec aperture on the original image was taken as the galaxy contribution f_g. We list these fluxes, corrected for foreground Galactic extinction, in Table 2.

We did not have *R*1- and *I*-band images available to measure the galaxy contribution by decomposition as above, so the galaxy contribution in these bands were estimated by extrapolating from the galaxy contribution measured in the SDSS-*i* band. The fluxes in Table 2 are in good agreement with those found by Salvati et al. (1993) and also agree well with the galaxy-subtracted *V*-band light curve published by Suganuma et al. (2006). We show in Fig. 3 the measured galaxy fluxes, converted to F_λ units and corrected for the small amount of foreground Galactic extinction towards the source. It is shown together with a template spectrum of the central regions of a normal spiral galaxy similar to NGC 4051 (Santos et al. 2002; Bica 1988). The template spectrum was constructed from a group of 30 galaxies, mostly of morphological type Sb, but also including Sa and Sc galaxies. NGC 4051 is classified as an Sbc galaxy. The template is corrected for Galactic extinction and normalized at 5870 Å. Our galaxy fluxes agree well with the template spectrum, indicating that our f_g measurements are good

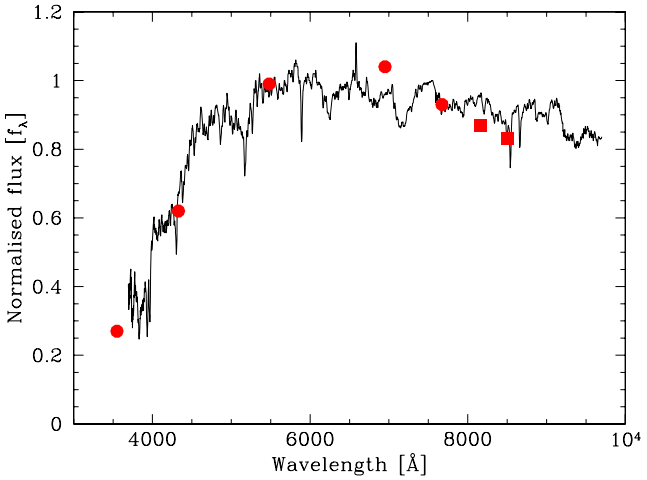

Figure 3. Measured galaxy flux inside the aperture (plotted in dots), compared to a template spectrum of the central regions of a normal spiral galaxy similar to NGC 4051. The last two points, plotted in squares, are the flux estimates for the *R*1 and *I* bands. These points were extrapolated from the SDSS-*i* flux measurement (last dot), as we did not have images available in these bands.

estimates of the host galaxy flux inside the aperture. Flux–flux plots between galaxy-subtracted light curves in different energy bands suggest that the error on f_g is between 10 and 15 per cent.

2.6 Fractional variability

The fractional variability $F_{\rm var}$ describes the flux variance of the light curve as a fraction of the mean flux $\langle f \rangle$ and provides a way of comparing the amount of intrinsic variability in each wavelength band. Mathematically,

$$F_{\rm var} = \frac{\sqrt{\sigma^2 - \langle \varepsilon^2 \rangle}}{\langle f \rangle}\,. \tag{1}$$

Here, σ is the flux variance:

$$\sigma^2 = \frac{1}{N}\sum_{i=1}^{N}(f_i - \langle f \rangle)^2 \tag{2}$$

and $\langle \varepsilon^2 \rangle$ is the mean of the squared measurement errors:

$$\langle \varepsilon^2 \rangle = \frac{1}{N}\sum_{i=1}^{N}\varepsilon_i^2. \tag{3}$$

The error on $F_{\rm var}$ is given by

$$\varepsilon_{(F_{\rm var})} = \sqrt{\left(\sqrt{\frac{1}{2N}}\,\frac{\langle \varepsilon^2 \rangle}{\langle f \rangle^2 F_{\rm var}}\right)^2 + \left(\sqrt{\frac{\langle \varepsilon^2 \rangle}{N}}\,\frac{1}{\langle f \rangle}\right)^2} \tag{4}$$

(Vaughan et al. 2003). This error describes only the error on $F_{\rm var}$ due to observational noise. In our case, there is also an uncertainty associated with the galaxy subtraction. This uncertainty does not affect the scatter of the points in the light curve (since we are subtracting the same galaxy contribution to each flux measurement), so should not be included in the average error in equation (3). It should be accounted for in the error on $F_{\rm var}$ however, so we also include a third error term in the square root of equation (4) of the form $(F_{\rm var}\,\Delta\langle f \rangle/\langle f \rangle)^2$, where $\Delta\langle f \rangle$ is the error in the galaxy flux contribution.

The fractional variability, as well as the ratio of the maximum to minimum flux in each light curve, is given in Table 2. We also list the variability characteristics of the 5100 Å continuum light curve together with the galaxy contribution measured by Bentz et al. (2009), but point out that this light curve was made using a smaller aperture than our light curves and that the galaxy contribution was measured from much higher resolution images than we used here. There may therefore be a difference in the amount of host galaxy flux subtracted, so the fractional variability in this band should not be compared directly with the other light curves. The X-ray and optical light curves are all highly variable. In agreement with the finding of Shemmer et al. (2003) that the optical continuum variations are less than the X-rays on time-scales of months, we find that the same is true on time-scales of years. The optical continuum (all light curves, including the 5100 Å light curve) is less variable than the X-rays, even after correcting for host galaxy starlight in the aperture.

In the X-ray reprocessing scenario, the fast variations of the X-ray light curve are smoothed out by the disc, so a smaller fractional variation of the optical light curves is expected. Our results are broadly consistent with this expectation, showing a decrease in $F_{\rm var}$ towards longer wavelengths. However, due to the uncertainty in the galaxy subtraction, the error on $F_{\rm var}$ is large, and the decreasing trend is not strong. The observation that the variability of the optical bands is less than that of the X-rays is nevertheless robust. We note that the variability of the *B*-band light curve is lower than the other optical bands and does not follow the decreasing trend. The mean flux of the galaxy-subtracted *B*-band light curve is also slightly higher than that of the *V* band, which is contrary to expectation, assuming that the emission in both bands originates in an accretion disc. This suggests that the low fractional variability in the *B* band may be the result of underestimating the galaxy contribution in this band. Increasing the galaxy contribution by 20 per cent increases $F_{\rm var}$ to 15.5 ± 1.3 per cent. The larger error may be attributed to the fact that the galaxy spectrum rises steeply in the *B* band (see Fig. 3) and is likely to be very different from the spectrum of the comparison star used in the differential photometry. The lower variability of the optical with respect to the X-ray variations suggests that reprocessing of X-rays may account for the optical variability in this source. We return to this possibility in Section 5.

3 THE OPTICAL POWER SPECTRUM

Power spectra are a commonly used technique to investigate the aperiodic variability displayed by AGN and X-ray binaries. It describes the variability power present in the light curve (mean squared amplitude) as a function of frequency. Generally, the X-ray power spectral density (PSD) of these systems can be described by a power law $P(\nu) \propto \nu^{-\alpha}$ of slope $\alpha \sim 1$ up to a bend or break frequency $\nu_{\rm B}$, where the power-law slope steepens to $\alpha \sim 2$ (e.g. McHardy et al. 2004; Summons 2008). The corresponding break time-scale scales approximately linearly with the black hole mass, and the scatter in this relationship is largely accounted for by considering the difference in the accretion rates between these systems (McHardy et al. 2006). The break frequency is thus characteristic of the system and is thought to represent a time-scale associated with the inner edge of the disc.

We use the Monte Carlo technique of Uttley, McHardy & Papadakis (2002) and Summons (2008) to estimate the parameters of the power spectrum underlying the optical variations. The method subtracts the mean of each of the component light curves and then calculates the discrete Fourier transform of each part. The resulting PSD is binned logarithmically in bins of a width of 1.5ν, with ν being the frequency at the start of the bin.

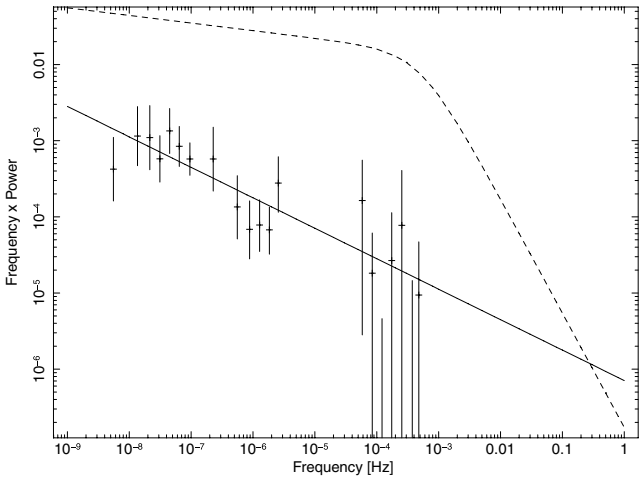

Figure 4. Unbroken power-law model (solid line) fitted to the unfolded optical PSD (points with error bars). The slope of the best-fitting model is $\alpha = 1.4$. The shape of the X-ray power spectrum (Summons 2008) is shown as a dashed line for comparison.

We do not include the AGN Watch data here, as the slightly different wavelength will affect the normalization of the power and hence the slope we measure. To extend the frequency range, we also include the V-band light curve obtained by Klimek et al. (2004) as part of their microvariability study. We calculate the variability power on each of the five nights it was observed and bin the resulting PSDs together to give the power in the frequency range of 6×10^{-5}–5×10^{-4} Hz. The low-frequency part of the PSD is calculated from the whole of the V-band light curve and the middle range from the most intensively sampled part of the light curve from MJD 54181 to 54252.

We start by fitting an unbroken power law

$$P(\nu) = A\nu^{-\alpha} \tag{5}$$

to the power spectrum, allowing the slope α and the normalization A to vary. The best fit, shown in Fig. 4, is found to have $\alpha = 1.4^{+0.6}_{-0.2}$, with an acceptance probability of 79.5 per cent. We also include the shape of the X-ray power spectrum, plotted as a dashed line, for comparison. The X-ray power spectrum has a slope $\alpha_{\rm L} = 1.1^{+0.1}_{-0.4}$ at low frequencies, bending to a slope of $\alpha_{\rm H} = 2.5^{+0.0}_{-0.8}$ and a frequency $\nu_{\rm B} = 5.1^{+4.9}_{-2.6} \times 10^{-4}$ Hz (Summons 2008; Summons et al., in preparation).

The unbroken optical PSD slope is intermediate in value between the low- and high-frequency X-ray slopes. If the optical PSD has a similar shape to the X-ray PSD, this suggests that a break is contained within the frequency range spanned by the optical data. Motivated by the shape of the X-ray PSD, we also fit a bending power law, of the form

$$P(\nu) = \frac{A\nu^{-\alpha_{\rm L}}}{1 + (\nu/\nu_{\rm B})^{\alpha_{\rm H}-\alpha_{\rm L}}} \tag{6}$$

to the optical PSD. For direct comparison with the X-ray PSD, we fixed the low-frequency slope to $\alpha_{\rm L} = 1.1$ and allowed the high-frequency slope $\alpha_{\rm H}$ and bend frequency $\nu_{\rm B}$ to vary. We find the best-fitting parameters to be $\alpha_{\rm H} = 1.5^{+1.0}_{-0.3}$ and bend frequency $\nu_{\rm B} = 1.4^{+*}_{-*} \times 10^{-8}$ Hz. The errors are the values for which the acceptance probability drops below 10 per cent and the asterisk is used to indicate an unbounded error. The acceptance probability for this fit is slightly better than for the unbroken case, at 90.2 per cent, but the break frequency is unconstrained by the frequency space sampled by the data. Allowing all the parameters to simultaneously vary over a large range (i.e. not fixing the value of the low-frequency slope) results in the same best-fitting values, within the quoted 90 per cent error bars.

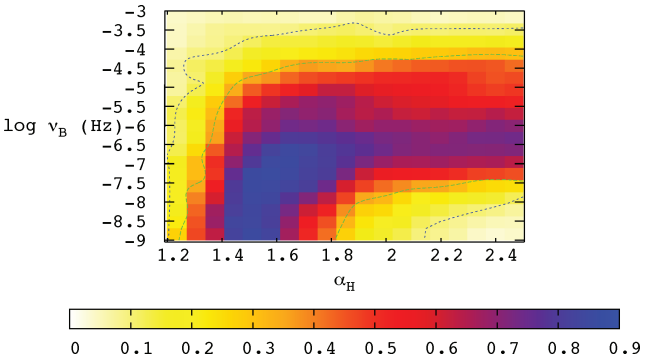

Figure 5. Acceptance probability as a function of $\alpha_{\rm H}$ and $\nu_{\rm B}$ for the parameter space searched. $\alpha_{\rm L}$ was fixed at 1.1, for direct comparison with the X-ray PSD. The best-fitting parameters yield an acceptance probability of 0.902. The lines superimposed on the colour plot are 67 and 90 per cent confidence contours.

We show in Fig. 5 a colour density plot of the acceptance probability as a function of the parameter space searched, while fixing $\alpha_{\rm L} = 1.1$. It shows that for $\alpha_{\rm H} = 2.5$, as measured from the X-ray spectrum, the best-fitting bend frequency is at $\nu_{\rm B} = 4.4^{+*}_{-4.2} \times 10^{-7}$ Hz. The fit probability for these parameters is only 74.7 per cent, however, so it can be confidently rejected in favour of the unbroken model. It is clear from this figure that the best-fitting bend frequency in the single-bend model is towards the lowest frequencies (longest time-scales) probed. A single-bend PSD cannot be ruled out for this system, but it would require further monitoring to confirm the existence of a bend at low frequencies. We therefore conclude that, with the current data, the optical power spectrum is best described by an unbroken steep power-law model with slope $\alpha = 1.4$.

4 CROSS-CORRELATION ANALYSIS

4.1 X-ray–optical correlation

In order to test whether there is a measurable delay of one light curve with respect to the other, we calculate their cross-correlation function (CCF), using the interpolation method of Gaskell & Sparke (1986) and White & Peterson (1994). We implement the method in two ways as follows. In the first case, we linearly interpolate between adjacent points and resample both light curves to obtain equally spaced points for calculating the correlation. We will refer to this method as the 'equally sampled' (EQ) method. We note, however, that for most of the monitoring time, the X-ray light curve is better sampled than the optical light curve. To take advantage of this and maximize the use of real, rather than interpolated data, we use a second implementation of the method, where we interpolate only the optical light curve and use the observed fluxes and observation times of the X-ray light curve in the calculation. We will designate this the 'single interpolation' (SI) method. The two methods give consistent results throughout, but for completeness we list the cross-correlation results from both methods in Table 3.

To take account of the gaps in the optical light curve when the galaxy is not observable from ground-based observatories, we divide the light curve into segments, defined by these gaps. We calculate the correlation between each segment and its corresponding

Table 3. Cross-correlation lags (in days). The centroid is the weighted average of the CCF values of ≥85 per cent of the peak correlation coefficient.

CCF X-ray versus	Peak (EQ)	Centroid (EQ)	Peak (SI)	Centroid (SI)
Optical[a]				
First peak	$2.0^{+1.2}_{-0.6}$	$2.4^{+0.9}_{-1.6}$	$1.2^{+1.0}_{-0.3}$	$1.8^{+1.3}_{-2.0}$
Second peak	$35.2^{+6.6}_{-5.1}$	$39.4^{+2.2}_{-2.1}$	$38.9^{+2.7}_{-8.4}$	$38.7^{+1.3}_{-1.0}$
u	$0.3^{+1.5}_{-1.3}$	$0.5^{+1.4}_{-1.6}$	$-0.2^{+1.6}_{-1.1}$	$0.1^{+2.0}_{-1.5}$
B	$2.3^{+1.5}_{-0.7}$	$2.6^{+0.5}_{-0.6}$	$1.5^{+0.8}_{-0.6}$	$2.0^{+0.8}_{-1.1}$
V	$1.1^{+0.5}_{-0.3}$	$2.2^{+0.3}_{-0.4}$	$0.6^{+0.4}_{-0.6}$	$1.3^{+0.8}_{-1.0}$
R	$3.1^{+1.0}_{-1.6}$	$2.8^{+0.6}_{-0.7}$	$1.5^{+1.6}_{-0.6}$	$2.0^{+0.9}_{-1.1}$
*R*1	$4.8^{+2.1}_{-3.3}$	$2.3^{+1.3}_{-1.7}$	$1.9^{+3.1}_{-1.0}$	$2.0^{+1.3}_{-2.2}$
I	$4.9^{+1.9}_{-2.4}$	$2.0^{+1.2}_{-1.9}$	$1.7^{+3.3}_{-0.8}$	$1.7^{+1.0}_{-1.7}$

[a]This is the light curve shown in Fig. 1, including both the *V*-band data and 5100 Å continuum AGN Watch data.

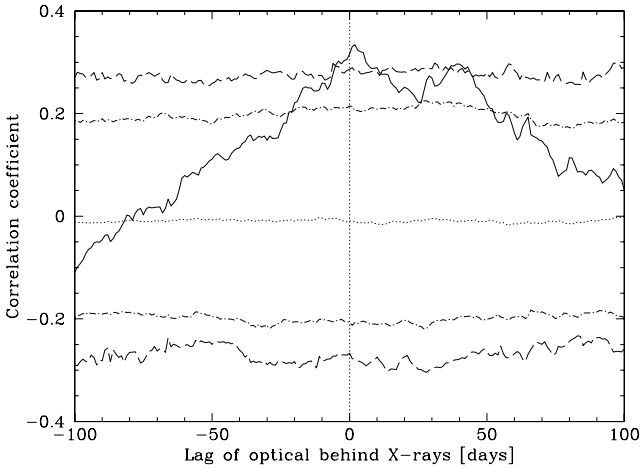

Figure 6. CCF between the X-ray and long-term optical light curves, shown in Fig. 1. The horizontal dotted, dot–dashed and dashed lines are the mean, 95 per cent and 99 per cent confidence levels, calculated from 1000 Monte Carlo simulations. The vertical dotted line indicates the zero lag position. Both the peaks are significant at greater than 99 per cent significance.

segment of the X-ray light curve and average the resulting CCFs, weighting them by the length (in time) of each segment. The final CCF, calculated in this way, is shown in Fig. 6. It shows a clear peak at $1.2^{+1.0}_{-0.3}$ d and another at $38.9^{+2.7}_{-8.4}$ d. The errors are calculated using a simple bootstrap method. We select at random two-thirds of the points in the X-ray light curve, each along with its closest optical data point, recalculate the CCF and then measure the peak and centroid. We performed 1000 such selections to yield a distribution of peak and centroid values. The error range reported contains 68 per cent of the measured values about the median. Here, and throughout this paper, a positive lag indicates the longer wavelength band lagging behind the shorter wavelength band.

The segmentation technique also allows us to take account of the small difference in the flux level of the *V* band and 5100 Å light curves due to different aperture sizes and a possible difference in the galaxy subtraction. The mean of each segment is calculated individually and subtracted from the segment before the correlation is calculated. The segmentation has the effect of removing long time-scale power in the light curve and allows a more accurate measure of the short time-scale lag between the light curves. Any

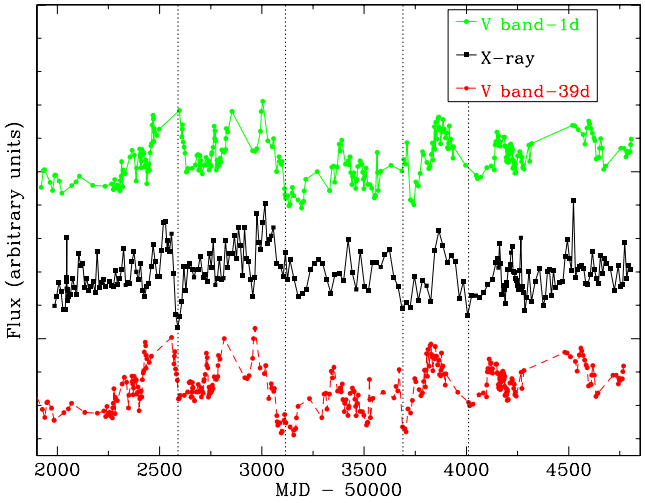

Figure 7. The optical *V*-band light curve shifted back by 1 d (top) and 39 d (bottom), compared to the X-ray light curve (middle). The X-ray light curve was binned in 5 d bins for clarity. The short time-scale correspondence between X-ray and the optical light curve at the top is clear. The vertical lines indicate some of the variations which align better when the optical light curve is shifted back by 39 d, rather than by the main 1 d lag.

small differences in the relative calibration of the light curves are therefore eliminated from the calculation.

We perform Monte Carlo simulations to test the significance of these lags in the following way: we generate 1000 random red noise light curves with the same statistical properties as the observed X-ray light curve, based on the method of Timmer & Koenig (1995) and the X-ray power spectrum parameters of NGC 4051 (Summons 2008; see also Section 3 of this paper). Each of these random, uncorrelated light curves is then sampled in the same way as the observed X-ray light curve and cross-correlated with the real, observed optical light curve, using the same segmentation technique as described above. The resulting CCF is recorded in each case and compared with the CCF of the observed light curves. In this way we can assess the probability of finding spurious correlations, i.e. chance correlations due to the red noise character of the light curves, that are higher than those of the real light curves. We overlay the mean, 95 per cent and 99 per cent levels of these simulations on top of the calculated CCF, in Fig. 6. Both peaks reach higher than the 99 per cent line, showing that the correlations are significant at greater than 99 per cent confidence.

To illustrate the origin of the two lags in the light curves, we show in Fig. 7 the optical light curve shifted by 1 (top) and 39 d (bottom) in comparison to the X-ray light curve (middle). The X-ray light curve was binned in 5 d bins for clarity. Most of the X-ray variations on time-scales of days to weeks show corresponding variations in the optical light curve shifted by 1 d. However, a few of the minima and maxima align better with the 39 d shifted version of the optical light curve. We point out that since both lags are short compared to the total duration of the light curve, only the largest amplitude variations can be clearly seen in Fig. 7. The most obvious examples of the delayed variations are marked by dotted lines in that figure.

4.2 Lags between optical bands

It is clear from the light curves in Fig. 2 that a strong correlation exists between the optical bands. Optical interband lags in this source have been measured by Sergeev et al. (2005) and Cackett

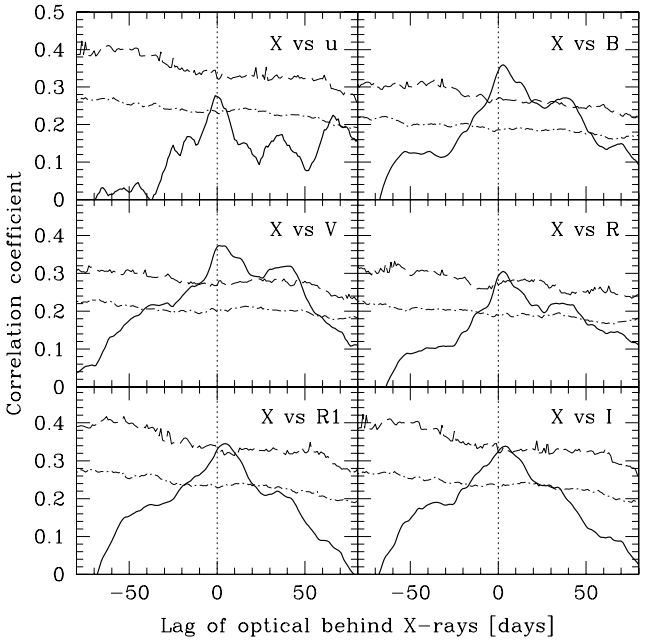

Figure 8. CCF between the X-ray and optical bands as labelled. The vertical dotted line indicates the zero lag position. For simplicity, we only show the 95 per cent (dot–dashed line) and 99 per cent (dashed line) confidence levels.

et al. (2007), confirming the apparent correlation. We consider here the relationship between the X-rays and each of the optical bands.

Using the same segmentation technique as before, we calculate the correlation between the X-ray light curve and each of the different optical bands. The CCFs are shown in Fig. 8 and we summarize in Table 3 the value of the peak and centroid of the CCF, calculated with both methods of interpolation. The centroid is calculated as the weighted average of the CCF points around the peak, at a value of $\geq$85 per cent of the peak correlation coefficient. As before, a positive value of the lag indicates that the variations in the optical band are lagging behind the X-ray variations. All light curves, except the *u* band, for which the sampling is much sparser than the other light curves, show a correlation significant at greater than 99 per cent confidence. The second peak near $\sim$40 d is also seen though not always at a significant level. We note, however, that the strength of the second peak, *relative* to the peak at $\sim$0 d, remains approximately constant. The *V*-band light curve used in this part of the analysis consists of only those observations which overlap in time with the other colour light curves. From this segment of the data we measure a slightly shorter lag than from the full light curve, but the results are consistent within the 1σ errors. We also note that the lags measured from the central CCF peak are well within the $\sim$6 light-day estimate of the location of the Hβ BLR in this source (Kaspi et al. 2000; Peterson et al. 2000, 2004), indicating that most of the variable optical emission originates in a structure smaller than the BLR.

In order to assess the influence of the delayed line emission on the measured lag, we first estimate the line contribution to the flux measured through the broad-band filters. Using an average optical spectrum from the AGN Watch programme, convolved with the filter response, we find a 3 per cent line contribution to the *V*-band flux and a 4 per cent contribution to the *B*-band flux. We then generate correlated X-ray and optical light curves, using the method described in Section 4.1, to represent the continuum emission. The line flux is represented as a smoothed version of the X-ray light curve, delayed by 6 d, as would be appropriate for a thin spherical shell of a radius of 6 light-days. The delayed line flux is added to the simulated, undelayed optical light curve in the ratios measured from the spectrum. 1000 such simulations yield a peak lag of $\tau_{\rm peak} = 0.0 \pm 0.1$ d and a centroid lag of $\tau_{\rm cent} = 0.1 \pm 0.6$ d, which is well within the errors on the lag measured in the real light curve. We therefore conclude that the line emission contributes too small a fraction of the total *V*-band emission to noticeably affect the measured lag.

5 REPROCESSING

The short, but measurable delays between the X-rays and the optical bands, as well as the small amplitude of the optical variations, suggest that reprocessing of X-rays plays a role in producing the optical variations. To test this hypothesis, we use the observed X-ray light curve to construct a model reprocessed optical light curve, which we can compare to the observed optical light curve.

The model, described in detail by Kazanas & Nayakshin (2001), assumes that the disc temperature is determined by the combined effects of viscous dissipation in the disc and variable heating by an X-ray source at height h_x above the disc and on its axis of symmetry. The temperature of the disc is then given by

$$T(R,t) = \left[\frac{3\dot{M}c^2}{8\pi\sigma R_g^2}\frac{1}{R^3}\left(1-\sqrt{\frac{R_{\rm in}}{R}}\right) + \frac{(1-\mathcal{A})L_x(t)}{4\pi\sigma\left(h_x^2+R^2\right)}\cos\theta\right]^{\frac{1}{4}}, \quad (7)$$

assuming that each annulus of the disc emits as a blackbody. Here $\dot{M}$ is the disc accretion rate in kg s^{-1}, R the distance of the disc surface element from the centre, $R_{\rm in}$ the location of the inner edge of the accretion disc, $L_x(t)$ the variable X-ray luminosity, $\mathcal{A}$ the average disc albedo and θ the angle between the disc surface and the direction of the X-ray source. R, $R_{\rm in}$ and h_x are measured in units of the gravitational radius $R_{\rm g} = GM/c^2$, where M is the mass of the black hole in kg. The delay between the variations of different wavebands is then due to the difference in light traveltime to regions of the disc of different temperatures.

We show in Fig. 9 the lags predicted by this model, plotted as a dashed line, assuming $M = 1.91 \times 10^6\,{\rm M}_\odot$ (Peterson et al. 2004), $\dot{M} = 0.15\dot{M}_{\rm Edd}$ (Woo & Urry 2002), $R_{\rm in} = 6, h_x = 10, \mathcal{A} = 0.3$ and a constant X-ray luminosity of $L_x = 3 \times 10^{42}$ erg s^{-1} (Smith & Vaughan 2007). The points with error bars are the measured centroid lags (of the light curves shown in Fig. 2 versus the X-rays) as a function of wavelength. With the above fixed parameters, the irradiated disc model (equation 7) is not a particularly good fit although, as we show next, a much better fit can be obtained if we alter the parameters (e.g. decrease the mass or increase the accretion rate).

Note that both terms in equation (7) scale as $R^{-3/4}$ for large radii. 'Large' here implies $R \gg R_{\rm in}$ and $R \gg h_x$, since we can write $\cos\theta = h_x/(h_x^2 + R^2)^{1/2}$. Together with the assumption that the peak of the emission scales as $T \propto \lambda^{-1}$, and writing the delay between different bands as $\tau = R/c$, we obtain the well-known $\tau \propto \lambda^{4/3}$ relationship commonly quoted in the context of reprocessing models. [Of course, where the large radius assumptions break down the relationship between the lag and the emitted wavelength is somewhat modified; see also Gaskell (2008).] We show in Fig. 9 (dotted line) that a simple $\lambda^{4/3}$ model, fitted to the measured lags via an arbitrary scaling constant, fits the data well. The factor of $\sim$2 difference between the two curves can easily be accounted for within the uncertainties on the model parameters.

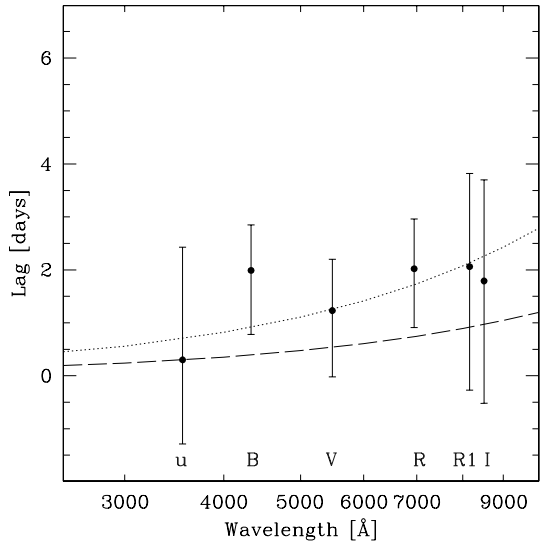

Figure 9. Centroid lags measured from the CCFs between the X-rays and optical colours. The dashed line shows the predicted lags from an irradiated accretion disc model for parameters appropriate to NGC 4051 (see text). The dotted line is a simple $\lambda^{4/3}$ model, fitted to the data by an arbitrary scaling constant.

To construct a model light curve, the emitted flux as a function of time may be computed by integrating the emission over all light traveltime delays τ to different parts of the disc, and throughout all disc radii,

$$f_\lambda(t) = \int_{R_{\rm in}}^{R_{\rm out}} \mathrm{d}R \int_{\tau_1}^{\tau_2} A(R,\tau) B_\lambda(T(R, t-\tau))\, \mathrm{d}\tau, \quad (8)$$

where $T(R,t)$ is given by equation (7). A is an area function obtained by considering the effect of the disc inclination on the distance between the X-ray source and the disc (see Berkley, Kazanas & Ozik 2000) and $B_\lambda(T)$ is the Planck function. $R_{\rm out}$ is a large value, appropriate for the outer edge of the disc.

We allowed the inner disc radius $R_{\rm in}$, the accretion rate $\dot{m} = \dot{M}/\dot{M}_{\rm Edd}$, height of the X-ray source h_x and disc inclination θ to vary, to find the parameters best describing the observed optical light curve. The mass was fixed at the reverberation-mapped value, $1.91 \times 10^6\,\mathrm{M}_\odot$ (Peterson et al. 2004).

Fig. 10 shows the observed optical light curve compared to a typical model reprocessed light curve. Due to the short light-traveltime to the optical emitting region, the rapid variability of the X-rays is preserved in the model light curves and we find that a range of input parameter values produce nearly identical model light curves. As expected, the model reprocessed light curve is highly correlated with the X-ray light curve, trailing it by 0.4–0.8 d, depending on the input parameters.

This is a very simple model, which assumes the X-rays to be emitted by a compact source located on the symmetry axis of the system, at a height h_x above the disc surface. In reality, it is more likely that the X-rays come from an extended corona. The compact source model used here may be viewed as a first-order approximation of the centroid of such a corona. We believe that this simplified model is sufficient in this case, as h_x is much smaller than the radius where most of the optical emission is coming from. The break in the X-ray power spectrum, which is thought to be associated with the inner edge of the disc, corresponds to the dynamical time-scale at $35R_{\rm g}$, or the viscous time-scale of a thick disc ($\alpha = 0.1$, $H/R \sim 0.5$) at $3R_{\rm g}$, so the bulk of the X-rays is probably emitted within a

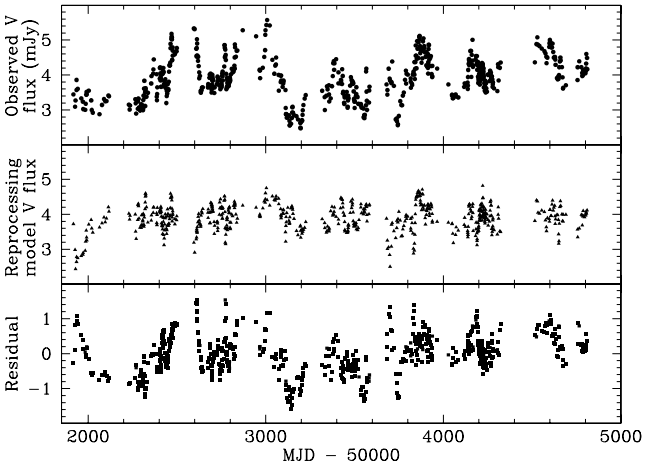

Figure 10. Top panel: galaxy-subtracted V-band light curve. Middle panel: best-fitting model reprocessed V-band light curve, using the observed X-ray light curve as input. Bottom panel: residual variations in the optical light curve after the reprocessed component has been removed.

radius smaller than, or comparable to, this. Using Comptonization models, Uttley et al. (2000) estimate the size of the emission region to be $<20R_{\rm g}$. Integrating the blackbody emission through the disc, we find that 95 per cent of the V-band emission originate from outside a radius of $400R_{\rm g}$. From this distance, even an extended corona would resemble a point source, making a more detailed model of the X-ray source unnecessary.

Reprocessing by a standard, thin disc appears to describe the observed lag and the short time-scale (approximately days) variations of the optical light curve well, but it fails to simultaneously reproduce the larger amplitude flares on time-scales of approximately months. Closer inspection of the light curves in Fig. 1 confirms that it is these larger amplitude fluctuations which lag the X-rays by $\sim$40 d (see e.g. MJD $\sim$ 50750, 52500 and 53700 for obvious examples). Attempting to isolate these variations, we show in the bottom panel of Fig. 10 the residual of subtracting the reprocessing model light curve from the observed light curve. Cross-correlation of the X-rays with this 'residual curve' yields the CCF shown in Fig. 11. As the model light curve is very well correlated with the X-rays at near 0 d, subtracting it removes this correlation peak entirely from the CCF (the correlation at this lag drops to zero). Isolating the second peak this way, allows us to make a more precise measurement of the lag it corresponds to. The peak is found to be at $38.9^{+1.2}_{-3.3}$ d and the 85 per cent centroid at $38.5^{+2.5}_{-2.2}$ d. We calculate the significance of the correlation as before, by cross-correlating random red noise light curves with the difference light curve. It is found to be significant at 98.4 per cent confidence. It is therefore clear that reprocessing by a flat disc can only account for the short lags in the light curve and that the second peak must be produced by optical emission from a structure further out.

6 DISCUSSION

The detection of two significant peaks in the X-ray/optical correlation function suggests that the optical variability originates from more than one location in the system or through more than one process. In the previous section, we discussed the correlation at short lags in terms of reprocessing by an accretion disc. We showed that this model can only reproduce the short time-scale variations in the

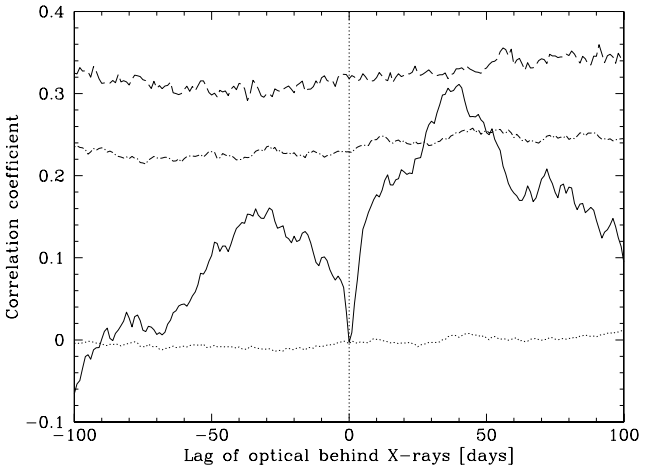

Figure 11. Cross-correlation of the reprocessing-subtracted residual light curve with the X-rays. The ∼0 d peak is removed entirely from the CCF, leaving only the longer time-scale correlation peak. The horizontal lines are the 50 per cent (dotted), 95 per cent (dot–dashed) and 99 per cent (dashed) significance levels. The peak is significant at 98.4 per cent.

light curve and that the second peak must be the result of optical emission coming from beyond the disc and BLR.

In this section, we investigate the origin of the second peak in the correlation function. The lag is found to be consistent with the light traveltime to the inner radius of the dust torus in this source, so we investigate the possibility of optical emission originating from the torus. First we will consider reprocessing of X-rays by the dust, and secondly the dust reflecting optical light from the accretion disc.

6.1 Second peak in the CCF – optical emission from the torus?

The standard model of AGN holds that the disc and BLR are surrounded by a large molecular torus. It is now widely accepted that the infrared emission from AGN is the result of reprocessing of high-energy radiation by hot dust in the torus (e.g. Glass 2004). We investigate here whether it is possible that the second peak detected in the correlation function could be the result of optical emission coming from the torus.

6.1.1 Distance to the torus

The inner radius of the dust distribution is set by the dust sublimation radius, inside which the flux from the central source will destroy the dust particles. Detailed radiative transfer calculations (Nenkova et al. 2008a) place this radius at

$$r_{\rm subl} = 0.4 \left(\frac{L}{10^{45}\,{\rm erg\,s^{-1}}} \right)^{0.5} \left(\frac{T}{1500\,{\rm K}} \right)^{-2.6} {\rm pc}, \qquad (9)$$

where T is the dust temperature and L the UV–optical luminosity.

Where adequate data exist, the optical-to-near-infrared delays show reasonable agreement with this model. Using both their own monitoring data and results from the literature, Oknyanskij & Horne (2001), Minezaki et al. (2004) and Suganuma et al. (2006) show that the optical-to-infrared lag is proportional to $L^{0.5}$ over a range of luminosities.

The exact temperature at which the dust in the torus sublimates is not well known, as it depends on the composition of the dust. The dust is generally assumed to be a mixture of graphite and silicate particles, with sublimation temperatures in the range of 1500–2000 K. The emission from hot dust at the inner edge of the torus is therefore expected to peak in the K band. As graphite can survive higher temperatures, it is assumed that the dust at the inner edge will mostly consist of graphite grains.

Gaskell (2007) pointed out that at such high temperatures, there must be a small, yet significant amount of optical emission coming from the torus as well, as part of the Wien tail of the ∼1500–2000 K emission. He proposed that the increase in time delay measured between the optical bands could be the result of contamination by the additional optical emission coming from large radii. Optical emission coming from the torus will of course also be delayed with respect to the X-rays by the same amount as the infrared emission. This will cause an asymmetry in the X-ray–optical correlation function, or, if the signal is strong enough, another peak may be seen, corresponding to the light traveltime to the inner edge of the torus. The dust recombination time-scale is expected to be long compared to the sublimation time-scale (Koshida et al. 2009) so that the inner edge of the torus is determined by the largest of the X-ray/UV flares. Any variations we see in the emitted flux is then probably due to temperature variations of the dust (below the sublimation temperature) rather than a change of the torus inner radius.

The $H - K$ colour measured for NGC 4051 by Suganuma et al. (2006) corresponds to a blackbody temperature of approximately 1600 K, so we adopt this value as the temperature of the dust in this source. We scale the ionizing X-ray-UV-optical luminosity (∼13.6 eV–13.6 keV), estimated by Ogle et al. (2004), to a distance of 15.2 Mpc, giving $L_{\rm ion} = 1.1 \times 10^{43}\,{\rm erg\,s^{-1}}$. The sublimation radius (equation 9) of NGC 4051 is then $r_{\rm subl} = 42.2$ light-days. The position of the second peak in our correlation function agrees well with this value. We note, however, that the V-to-K lag found by Suganuma et al. (2006) is only ∼20 light-days. This may be expected if the disc V-band emission is contaminated by optical emission from large radii (such as the torus), as this will shift the peak of the V versus K CCF to shorter lags. Several studies (Kaspi et al. 2000; Peterson et al. 2000, 2004) measure the location of the BLR to be at ∼6 light-days, placing even the smallest estimates of the torus well outside the disc and BLR.

6.1.2 Energetics

Detailed models of AGN dust tori (e.g. Nenkova et al. 2008a,b) take account of the fact that the torus probably consists of clumpy material rather than a smooth distribution of dust. One effect the clumps has is to cause a steep radial temperature gradient in the torus, as optically thick clouds closer to the source can shield those further away from direct irradiation. It also takes into account the diffuse heating of clumps by each other. Such a detailed analysis is beyond the scope of this paper, but as we are mainly interested in the hottest dust here, a simplified approach may be sufficient to determine whether it is energetically possible to get the 1–2 mJy V-band flux required to explain the large amplitude optical fluctuations, from the torus.

A blackbody at 1600 K emits roughly 16 per cent of its total emission in the K band and only 0.04 per cent in the Wien tail at V-band wavelengths. The fraction of V-band emission decreases very rapidly as the dust temperature decreases, so we do not expect to find a significant contribution to the optical from further into the torus. We will assume that the optical emission is identified with the inner edge of the dust distribution only, where the hottest dust is located. For simplicity, we also assume a sharp boundary, although the transition is most likely a gradual one,

given the difference in sublimation temperatures of different dust particles. We follow the prescription of Barvainis (1987) to calculate the luminosity emitted by the dust. We assume a grain radius of $a = 0.05\,\mu$m and infrared (K-band) absorption efficiency $Q_{\rm abs} = 0.058$. The luminosity of a single grain is given by $L_\nu^{\rm gr} = 4\pi a^2 \pi Q_\nu\, B_\nu(T)\,{\rm erg\,s^{-1}\,Hz^{-1}}$, where B_ν is the Planck spectrum of a grain at temperature T. The K-band spectral luminosity of a graphite grain at $T = 1600$ K is then $L_K^{\rm gr} = 3.6 \times 10^{-17}\,{\rm erg\,s^{-1}\,Hz^{-1}}$. The average galaxy-subtracted K-band flux measured by Suganuma et al. (2006) is 31 mJy, which corresponds to a total K-band luminosity of $L_K = 8.6 \times 10^{27}\,{\rm erg\,s^{-1}\,Hz^{-1}}$. Hence, the total number of hot dust grains is $N \sim 2.4 \times 10^{44}$. For UV–optical radiation, the absorption efficiency is $Q_{\rm abs} \sim 1$ for grains of this size (Wickramasinghe, Lukes & Dempsey 1974). The optical emission of a grain at 1600 K is $L_V^{\rm gr} = 1.9 \times 10^{-19}\,{\rm erg\,s^{-1}\,Hz^{-1}}$. If we assume the same number of grains to be emitting this optical emission (i.e. only the hottest dust), then the total V-band luminosity we may expect from the torus is $L_V = 4.4 \times 10^{25}\,{\rm erg\,s^{-1}\,Hz^{-1}}$. This translates to an observed flux of only 0.16 mJy, which is an order of magnitude smaller than required to explain the additional variability in the observed V-band light curve.

One of the main uncertainties in this model is the dust composition, as there is no guarantee that dust in the vicinity of the active nucleus will be the same as dust found in molecular clouds. The temperature of the grains is determined by the balance between UV absorption and infrared emission, which vary with the grain size and type. This, in turn, affects the sublimation temperature. If we allow the dust temperature to increase to 1800 K (which is still within the range of the sublimation temperature of graphite), the emitted luminosity per grain increases to $L_V^{\rm gr} = 1.15 \times 10^{-18}\,{\rm erg\,s^{-1}\,Hz^{-1}}$ and the additional flux observed in the V band to 1.1 mJy. Such an increase in the temperature the dust particles can sustain will of course move the sublimation radius inwards as well, to a distance of $r_{\rm subl} = 31.1$ light-days. This is within the 1σ error of the peak measured on the X-ray–optical CCF (Fig. 6) and within 2σ of the peak measured from the CCF calculated using the residual light curve (Fig. 11). The uncertainty on $L_{\rm ion}$ would also allow a factor of $\sim$2 change in the sublimation radius.

A similar analysis for the other optical bands, using $T = 1800$ K and the appropriate absorption efficiencies, yields $u = 0.004$, $B = 0.08$, $R = 5.8$, $R1 = 13.2$ and $I = 16.6$ mJy. For wavelengths R and longer, the reprocessing model therefore predicts a higher flux to come from the torus alone than the total galaxy-subtracted flux we measure. The measured fluxes in these bands must, however, include a significant contribution from the disc as well, as their correlation functions with the X-rays (Fig. 8) all display a significant peak at short lags.

For increasing wavelength, the torus reprocessing model naturally predicts an increase in the amount of reprocessed flux originating in the torus, as the redder bands include a larger fraction of the total flux emitted by the dust. Our data do not appear to support such an increase, so it is unlikely that all the additional optical flux results from dust reprocessing. We nevertheless cannot exclude the possibility that some of the optical emission in this source is originating in the dust torus.

6.1.3 *Optical reflection*

In this section, we consider the reflection of optical light by the torus. Apart from the illumination by the central source, the torus will also receive UV and optical light from the accretion disc. The dust absorbs energy at these wavelengths very efficiently, so some of this reprocessed optical emission will be absorbed by the dust and contribute to the variable heating of the torus, as discussed in the previous section. Depending on the solid angle subtended by the torus at the optically emitting part of the disc, some of the optical emission may also be elastically scattered and reflected by the torus. The efficiency of reflection is strongly geometry dependent, so we will limit our discussion here to a qualitative description of the main observable results expected. Reflection from different geometries have been considered by Goosmann & Gaskell (2007) in the development of their Monte Carlo polarization code STOKES.

Most of the UV/optical illumination will be relatively steady or will vary on the very long (years) viscous time-scales on which the intrinsic emission from the disc will vary. However, as we have already shown, a small fraction of the optical illumination, resulting from reprocessing of X-rays by the accretion disc, will follow the pattern of the X-ray variations. As the optically emitting region is about a light-day away from the central X-ray source, the torus will see optical emission which broadly follows the X-ray emission, but which is smoothed on a time-scale of a day or two relative to the X-ray variability pattern.

The component of the optical emission illuminating the torus, which has a phase relationship with the X-rays (so that it causes a peak in the CCF), must have arisen from reprocessing of X-rays in the disc. The amount of scattered light depends on the solid angle the torus subtends at the optically emitting part of the disc, so for large solid angles, the elastically scattered optical photons may produce a noticeable contribution to the optical variations and will lag the X-rays by about 40 d. Dust models by Draine (2003) suggest that the scattering albedo (scattering cross-section as a fraction of the total extinction cross-section) of Milky Way type dust may be as high as 0.5–0.8, for different dust compositions. Dust in AGN probably consists of larger grains (smaller grains are evaporated by the intense radiation field), so the albedo is uncertain, but it may still be high enough for the scattered light to contribute significantly to the observed optical radiation.

Reflection models are supported by spectropolarimetric studies which are used to detect the BLR in Seyfert 2 galaxies, such as NGC 1068, through polarized light. In these systems, the continuum source and BLR clouds are hidden from our view by the molecular torus, but their emission is scattered into our line of sight by warm electrons and dust lying outside the torus opening, polarizing the light. In Seyfert 1 galaxies, however, the optical polarization position angle is generally observed to be parallel to the radio axis (which is assumed to be the system axis), suggesting that the scattering medium has an equatorial geometry, perhaps a ring of material co-planar with the accretion disc (Smith et al. 2002, 2004), or the inner edge of the torus (Cohen & Martel 2002). The optical continuum polarization in NGC 4051, as measured by Smith et al. (2002), is low however. They find 0.5 per cent of the optical continuum at 7000 Å to be polarized, amounting to a mere $\sim$0.05 mJy. It is also not clear to what extent this is intrinsic to the source or whether the measurement is contaminated by foreground interstellar polarization. If intrinsic, the position angle of the polarization is approximately parallel to the radio axis, suggesting that the scattering occurs in the equatorial region. Unfortunately, their polarization observation was made during a time for which we do not have optical monitoring data available, so we cannot comment on the general optical behaviour of the source at that time.

There is also evidence for diffuse continuum emission and reprocessing by the BLR as well as reflection by the broad-line clouds

(Korista & Ferland 1998; Korista & Goad 2001; Arévalo et al. 2009) in some Seyfert galaxies. However, as mentioned before, any lags associated with the BLR (∼6 d for NGC 4051) are likely to be much shorter than those associated with the torus.

As an aside, we note that the high-energy emission may also be reflected by the torus. X-ray spectra show evidence of X-ray reflection by high density gas in the form of the 'Compton bump' and the Fe Kα fluorescence line at 6.4 keV. This line is thought to originate in the accretion disc and is therefore expected to be broadened by relativistic Doppler motions. Broad Fe lines like this are seen in X-ray spectra, but the line is found to have a narrow component as well, which is associated with reflection by distant, optically thick material such as the molecular torus (e.g. Nandra et al. 2007).

Neither the reprocessing nor the scattering model can on its own fully account for the optical flux causing the second peak in the correlation function, but it is possible that either or both may contribute to the optical emission observed from the system. Overall, we conclude that there are many possible sources of optical emission in the inner parts of AGN but all those associated with the torus, albeit reprocessing or simple reflection, will give more or less the same lag. Our current data are not suited to constrain these models further, so a more detailed discussion is beyond the scope of this paper.

6.2 The complex optical variability in NGC 4051

Shemmer et al. (2003) find that part of the optical emission leads the X-ray variations by approximately 2 d, contrary to what we find here (see Table 3). As was shown in previous sections, there is more than one effect contributing to the optical variations in this source. Variations on time-scales longer than, or similar to, their 3 month monitoring period may cause asymmetries in the correlation function and hence a centroid at negative lags. Shemmer et al. (2003) interpret their result as a combination of reprocessing and longer time-scale variations, similar to what we find over much longer time-scales. We note that the peak of their CCF is consistent with the peak lag we find here, ∼1 d.

In red noise time series, such as the X-ray and optical light curves used here, peaks and troughs may sometimes line up even if the light curves are not really correlated, producing spurious peaks in the CCF. We believe that the second peak we measure in the CCF here is not simply due to statistical fluctuations like these, as it is present in most of the individual segments used to calculate the final CCFs. If this was an effect only due to a random correlation in a red noise process, we would expect to see it in, e.g., only one of the segments' CCFs. We note that the peak does shift between ∼30 and 50 d in the CCFs of the different segments. The probability that the peak is due to such statistical fluctuations was assessed through Monte Carlo simulations in Section 4 and was found to be 1.6 per cent.

So far, we have interpreted the second peak in the CCF only in terms of a light crossing time-scale. Other time-scales of interest are the dynamical (Kepler) time-scale and the viscous time-scale, on which we expect accretion rate fluctuations to propagate through the disc. A lag of the optical variations behind the X-rays, as seen here, would require such fluctuations to be propagating outwards through the disc for this time-scale to be relevant. A viscous time-scale of 40 d corresponds to $R = 50R_{\rm g}$ in a moderately thin, optically thick disc ($H/R \sim 0.1$, $\alpha_{\rm disc} = 0.1$) or to $R = 440R_{\rm g}$ in a geometrically thick disc ($H/R \sim 0.5$, $\alpha_{\rm disc} = 0.1$). $R = 50R_{\rm g}$ lies well within the far-UV to EUV emitting part of the disc; less than 0.5 per cent of the optical emission come from within this radius. $R = 440R_{\rm g}$ contains approximately 6 per cent of the optical emission. Enhanced emission due to viscous instability in this region could therefore only cause an ∼6 per cent variation in the light curve. This translates to a flux variation of 0.2 mJy, which is not enough to explain the variations seen in the light curve. As an orbital time-scale, 40 d corresponds to the radius which contains 69 per cent of the V-band emission, but it is difficult to associate an orbital time-scale with a lag between the emission in different wavebands, as we see here.

If this is indeed optical emission from the torus, why has this not been seen in other sources? NGC 4051 is a low mass, low-luminosity system, which means that it is physically smaller than higher mass AGN. Lags between the optical and near-infrared suggest that dust sublimation radii in most sources are several tens to hundreds of days, but here it is only ∼20–40 d. The optical emission from the torus will be a very weak signal, so long enough light curves are necessary to include several cycles of the correlated variations to produce a significant peak in the CCF. We note that calculating the CCF using only half of the V-band data decreases the significance of the second peak in Fig. 6 to 96.3 per cent or to below 95 per cent if only a quarter of the light curve is used.

More importantly, in low mass systems the V-band emission originating in the torus is probably a larger fraction of the total V-band emission emitted by the system than it is in more massive systems. This is due to the variation in disc temperature with black hole mass. For example, for a fixed accretion rate of $\dot{m} = 0.10$, a standard disc (e.g. Frank, King & Raine 2002) around a $10^8\,{\rm M}_\odot$ black hole emits 1.9 per cent of its total luminosity at V-band wavelengths, but for a $10^6\,{\rm M}_\odot$ black hole the disc is hotter, the bulk of the energy is emitted at bluer wavelengths and the fraction of the total emission emitted at V-band wavelengths decreases to 0.4 per cent. On the contrary, the torus in all sources is expected to be at approximately the same temperature (as its inner radius and temperature are determined by dust sublimation) and hence it will contribute a constant fraction of the V-band emission. Comparing this constant fraction with the V-band emission originating in the disc, the torus contributes a larger fraction to the total V-band emission in the $10^6\,{\rm M}_\odot$ source than it does in the $10^8\,{\rm M}_\odot$ source. In more massive systems the V-band emission is therefore dominated by the disc, so the weak optical emission from the torus will be very hard to isolate.

Long-term multicolour optical and infrared monitoring of NGC 4051 is needed to reliably measure the inner radius of the dust torus and the possible contribution of the disc to the near-infrared (e.g. Tomita et al. 2006). Detailed modelling of the torus emission, taking into account both the geometry of the system and the dust albedo and emission properties, is also necessary to properly assess the contribution this could have to the optical emission observed.

7 SUMMARY

We have presented a 12.6 year 3–10 keV X-ray light curve from our ongoing long-term X-ray monitoring programme on *RXTE*, along with concurrent optical monitoring light curves. We combined the V-band data from four different telescopes with archival 5100 Å continuum data, to construct an optical light curve spanning the same length in time. We also include light curves in the u, B, R, $R1$ and I optical bands, each of length between 3.6 and 6.6 years in time.

We find both the X-ray and optical emission to be highly variable, but find the amplitude of the optical emission to be smaller than that of the X-rays, even after subtracting the contaminating host galaxy flux falling inside the aperture. The power spectra show that the

optical variability power is lower than the X-rays on all time-scales probed. With the current data, the optical PSD is best described by an unbroken power law of slope $\alpha = 1.4$, which is much steeper than the low-frequency slope of the X-ray PSD ($\alpha_{\rm L} = 1.1$). This suggests that the variations in the different bands do not have a common origin or that they are not related in a simple way. We will address this issue in more detail in a future paper.

We measured the galaxy flux inside the 15 arcsec aperture by decomposition of the optical images and found the measured fluxes to agree well with a template spectrum of a similar non-active spiral galaxy.

The CCF between the optical light curve and the X-rays displays two statistically significant peaks. The strongest peak corresponds to the optical variations lagging the X-rays by $1.2^{+1.0}_{-0.3}$ d. This time-scale is consistent with the light traveltime to the optical emitting region of the accretion disc and points to X-ray reprocessing as the source of the fast optical variations. The delays measured between other optical colours and the X-rays are also consistent with this interpretation. However, using a reprocessing model, we find that all the optical variability cannot be accounted for this way. Reprocessing appears to describe the small amplitude, fast variations well, but it fails to reproduce the larger amplitude variations on time-scales of months to years that are also seen in the light curve.

The second significant peak in the CCF is at an optical lag of $38.9^{+2.7}_{-8.4}$ d behind the X-rays. By subtracting a model reprocessed light curve from the observed optical light curve and recalculating the cross-correlation, we can constrain this peak more precisely, namely $38.9^{+1.2}_{-3.3}$ d. Interpreting this as a light traveltime, the corresponding radius is consistent with the dust sublimation radius in this AGN, which is a theoretical estimate of the inner radius of the dust torus.

As such, we have investigated the origin of the additional optical emission, both in terms of a weak optical contribution from X-ray reprocessing by the dust and in terms of reflection of optical light from the disc by the dust. We find that neither process can on its own explain the origin of the second peak in the CCF of NGC 4051. It remains possible, however, that both these processes may contribute to the optical emission observed. Detailed modelling of the dust emission properties at optical wavelengths as well as further optical polarimetry will be required to thoroughly test this hypothesis.

In general, the weak (though significant) short time-scale correlation reported here is consistent with a model where the strength of the correlation is determined by the mass of the central black hole and disc accretion rate (Uttley et al. 2003). When scaled in terms of gravitational radius, a standard accretion disc (e.g. Shakura & Sunyaev 1973) around a smaller mass black hole, with a given accretion rate, is hotter. The optical emitting region will therefore be further away from the centre and the viscous time-scale here will be much longer than near the centre, where the X-rays are emitted. The variations in the different bands may therefore be expected to vary incoherently, weakening the strength of the correlation. Furthermore, the mass dependence of the disc temperature may also explain why an optical contribution from the torus is detected in this source and not in more massive systems: the cooler discs around more massive systems will emit most of their luminosity at optical wavelengths, dominating over the weak optical signal from the torus. In low mass systems with hotter discs, such as NGC 4051, the peak of the disc emission is shifted to shorter wavelengths, decreasing the fraction of the emission emitted at *V*-band wavelengths and hence increasing the possibility of detecting optical emission from the torus.

ACKNOWLEDGMENTS

We thank the referee for constructive suggestions which improved this paper.

We are grateful to the staff of the *RXTE*, the LT and the FT for their support of our long-term programme and also thank Keith Horne and Ed Cackett for their contribution in obtaining these data.

EB gratefully acknowledges financial support in the form of a Stobie-SALT Scholarship from South African National Research Foundation and the University of Southampton. IM$^{\rm c}$H acknowledges support from the STFC under rolling grant PP/D001013/1 and PA acknowledges support from the Natural Science Foundation of China (grants 10773024, 10833002, 10821302, 10825314, 10873030 and 40636031) and National Basic Research Program of China (grant 2009CB824800). PU acknowledges support from an STFC Advanced Fellowship. The work of SGS and NGC is partially supported by the CosmoMicroPhysics Target Complex Programme of the Ukrainian NAS.

REFERENCES

Arévalo P., Uttley P., 2006, MNRAS, 367, 801
Arévalo P., Uttley P., Kaspi S., Breedt E., Lira P., McHardy I. M., 2008, MNRAS, 389, 1479
Arévalo P., Uttley P., Lira P., Breedt E., McHardy I. M., Churazov E., 2009, MNRAS, 397, 2004
Barvainis R., 1987, ApJ, 320, 537
Bentz M. C., Peterson B. M., Netzer H., Pogge R. W., Vestergaard M., 2009, ApJ, 697, 160
Berkley A. J., Kazanas D., Ozik J., 2000, ApJ, 535, 712
Bica E., 1988, A&A, 195, 76
Breedt E. et al., 2009, MNRAS, 394, 427
Cackett E. M., Horne K., Winkler H., 2007, MNRAS, 380, 669
Chesnok N. G., Sergeev S. G., Vavilova I. B., 2009, Kinematics Phys. Celest. Bodies, 25, 107
Cohen M. H., Martel A. R., 2002, in Crenshaw D. M., Kraemer S. B., George I. M., eds, ASP Conf. Ser. Vol. 255, Mass Outflow in Active Galactic Nuclei: New Perspectives. Astron. Soc. Pac., San Francisco, p. 255
Collier S. J. et al., 1998, ApJ, 500, 162
Done C., Ward M. J., Fabian A. C., Kunieda H., Tsuruta S., Lawrence A., Smith M. G., Wamsteker W., 1990, MNRAS, 243, 713
Doroshenko V. T., Sergeev S. G., Merkulova N. I., Sergeeva E. A., Golubinsky Y. V., Pronik V. I., Okhmat N. N., 2005, Astrophysics, 48, 156
Draine B. T., 2003, ApJ, 598, 1017
Frank J., King A., Raine D. J., 2002, in Frank J., King A., eds, Accretion Power in Astrophysics, 3rd edn. Cambridge Univ. Press, Cambridge, p. 398
Gaskell C. M., 2007, in Ho L. C., Wang J.-W., eds, ASP Conf. Ser. Vol. 373, The Central Engine of Active Galactic Nuclei. Astron. Soc. Pac., San Francisco, p. 596
Gaskell C. M., 2008, Rev. Mex. Astron. Astrofis., 32, 1
Gaskell C. M., Sparke L. S., 1986, ApJ, 305, 175
Glass I. S., 2004, MNRAS, 350, 1049
Goosmann R. W., Gaskell C. M., 2007, A&A, 465, 129
Haardt F., Maraschi L., 1991, ApJ, 380, L51
Kaspi S., Smith P. S., Netzer H., Maoz D., Jannuzi B. T., Giveon U., 2000, ApJ, 533, 631
Kazanas D., Nayakshin S., 2001, ApJ, 550, 655
Klimek E. S., Gaskell C. M., Hedrick C. H., 2004, ApJ, 609, 69
Koratkar A., Blaes O., 1999, PASP, 111, 1
Korista K., Ferland G., 1998, ApJ, 495, 672
Korista K. T., Goad M. R., 2001, ApJ, 553, 695
Koshida S. et al., 2009, ApJ, 700, L109

Krolik J. H., Horne K., Kallman T. R., Malkan M. A., Edelson R. A., Kriss G. A., 1991, ApJ, 371, 541
Lyubarskii Y. E., 1997, MNRAS, 292, 679
McHardy I. M., Papadakis I. E., Uttley P., Page M. J., Mason K. O., 2004, MNRAS, 348, 783
McHardy I. M., Koerding E., Knigge C., Uttley P., Fender R. P., 2006, Nat, 444, 730
Maoz D., Edelson R., Nandra K., 2000, AJ, 119, 119
Maoz D., Markowitz A., Edelson R., Nandra K., 2002, AJ, 124, 1988
Mason K. O. et al., 2002, ApJ, 580, L117
Minezaki T., Yoshii Y., Kobayashi Y., Enya K., Suganuma M., Tomita H., Aoki T., Peterson B. A., 2004, ApJ, 600, L35
Nandra K., Le T., George I. M., Edelson R. A., Mushotzky R. F., Peterson B. M., Turner T. J., 2000, ApJ, 544, 734
Nandra K., O'Neill P. M., George I. M., Reeves J. N., 2007, MNRAS, 382, 194
Nenkova M., Sirocky M. M., Ivezić Ž., Elitzur M., 2008a, ApJ, 685, 147
Nenkova M., Sirocky M. M., Nikutta R., Ivezić Ž., Elitzur M., 2008b, ApJ, 685, 160
Ogle P. M., Mason K. O., Page M. J., Salvi N. J., Cordova F. A., McHardy I. M., Priedhorsky W. C., 2004, ApJ, 606, 151
Oknyanskij V. L., Horne K., 2001, in Peterson B. M., Pogge R. W., Polidan R. S., eds, ASP Conf. Ser. Vol. 224, Probing the Physics of Active Galactic Nuclei. Astron. Soc. Pac., San Francisco, p. 149
Oknyanskij V. L., Horne K., Lyuty V. M., Sadakane K., Honda S., Tanabe S., 2003, in Collin S., Combes F., Shlosman I., eds, ASP Conf. Ser. Vol. 290, Active Galactic Nuclei: From Central Engine to Host Galaxy. Astron. Soc. Pac., San Francisco, p. 119
Peng C. Y., Ho L. C., Impey C. D., Rix H.-W., 2002, AJ, 124, 266
Peterson B. M., 1999, in Gaskell C. M., Brandt W. N., Dietrich M., Dultzin-Hacyan D., Eracleous M., eds, ASP Conf. Ser. Vol. 175, Structure and Kinematics of Quasar Broad Line Regions. Astron. Soc. Pac., San Francisco, p. 49
Peterson B. M. et al., 2000, ApJ, 542, 161
Peterson B. M. et al., 2004, ApJ, 613, 682
Russell D. G., 2003, preprint (astro-ph/0310284)
Salvati M. et al., 1993, A&A, 274, 174
Santos J. F. C. J., Alloin D., Bica E., Bonatto C., 2002, in Geisler D. P., Grebel E. K., Minniti D., eds, Proc. IAU Symp. 207, Extragalactic Star Clusters. Kluwer, Dordrecht, p. 1
Sergeev S. G., Doroshenko V. T., Golubinskiy Y. V., Merkulova N. I., Sergeeva E. A., 2005, ApJ, 622, 129
Shakura N. I., Sunyaev R. A., 1973, A&A, 24, 337
Shemmer O., Uttley P., Netzer H., McHardy I. M., 2003, MNRAS, 343, 1341
Smith R., Vaughan S., 2007, MNRAS, 375, 1479
Smith J. E., Young S., Robinson A., Corbett E. A., Giannuzzo M. E., Axon D. J., Hough J. H., 2002, MNRAS, 335, 773
Smith J. E., Robinson A., Alexander D. M., Young S., Axon D. J., Corbett E. A., 2004, MNRAS, 350, 140
Steele I. A. et al., 2004, in Oschmann J. M., Jr, ed., Proc. SPIE 5489, Ground-Based Telescopes. SPIE, Bellingham, p. 679
Suganuma M. et al., 2006, ApJ, 639, 46
Summons D., 2008, PhD thesis, Univ. Southampton
Timmer J., Koenig M., 1995, A&A, 300, 707
Tomita H. et al., 2006, ApJ, 652, L13
Uttley P., McHardy I. M., Papadakis I. E., Cagnoni I., Fruscione A., 2000, MNRAS, 312, 880
Uttley P., McHardy I. M., Papadakis I. E., 2002, MNRAS, 332, 231
Uttley P., Edelson R., McHardy I. M., Peterson B. M., Markowitz A., 2003, ApJ, 584, L53
Vaughan S., Edelson R., Warwick R. S., Uttley P., 2003, MNRAS, 345, 1271
Wanders I. et al., 1997, ApJS, 113, 69
White R. J., Peterson B. M., 1994, PASP, 106, 879
Wickramasinghe N. C., Lukes T., Dempsey M. J., 1974, Ap&SS, 30, 315
Woo J.-H., Urry C. M., 2002, ApJ, 579, 530
Yoshii Y., Kobayashi Y., Minezaki T., 2003, BAAS, 35, 752

This paper has been typeset from a TEX/LATEX file prepared by the author.